Quantum optics with DNA encapsulated silver clusters on nanotubes

bachelorthesis

Irina Komen

July 5th, 2012

supervision:
Sumant Oemrawsingh
Nemanja Markešević
Dirk Bouwmeester

Quantum Optics & Quantum Information
University of Leiden

Contents

1 Introduction **4**

2 Theory **5**
2.1 DNA encapsulated silver clusters 5
2.2 Fluorescence 6
2.3 Single molecule spectroscopy 8
2.4 DNA tubes 8
2.4.1 DNA tubes with silver clusters 9
2.4.2 Quantum optics on DNA tubes 9
2.5 Photon statistics 9
2.5.1 Correlation functions 9
2.5.2 Bunching and antibunching 12
2.5.3 Experiment 12

3 Experimental methods **14**
3.1 Samples 14
3.2 Fluorimetry 14
3.3 Microscopy 14
3.4 Setup 14

4 DNA tubes **17**
4.1 Results 17
4.1.1 Fluorimetry 17
4.1.2 Microscopy 18
4.1.3 9C tubes 18
4.1.4 Tubes with other hairpins 20
4.2 Discussion 21
4.2.1 Tubes with other hairpins 21

5 Cryostat **23**

6 Spectral features **24**
6.1 Results 24
6.1.1 9C tubes spectra at room temperature 24
6.1.2 9C tubes spectra at cryogenic temperatures 25
6.1.3 9C hairpins spectra 27
6.1.4 Tubes with different silver concentrations 28
6.1.5 Intensities and linewidths 29
6.1.6 7C tubes spectra 29
6.1.7 Time traces 31
6.1.8 Photon statistics 32
6.2 Discussion 33
6.2.1 Time traces 33
6.2.2 Three peaks 33

6.2.3 Temperature dependence of intensity 34
6.2.4 Using intensity to determine hairpin amount 35

7 Conclusion **37**

A Recipes, procedures and materials **40**
A.1 Strand sequences 40
A.2 Recipes 40
A.2.1 FAM tubes 40
A.2.2 9C/7C/6CA2 tubes 40
A.2.3 9C 50% tubes 41
A.2.4 9C 25% tubes 41
A.2.5 9C hairpins 41
A.2.6 Silver reduction ratios 41
A.2.7 Imaging ratios 42
A.2.8 PVA concentrations 42
A.2.9 Intercalating dye 42
A.3 Procedures 42
A.3.1 Fluorimetry 42
A.3.2 Spin coating 43
A.3.3 Filtering 43
A.4 Specifications 43
A.4.1 Setup 43
A.4.2 Microscope 43

B Trials **44**
B.1 Filtering 44
B.2 Self-Assembly 44

C Tangles under the microscope **46**

1 Introduction

Silver nanoclusters bridge the gap between single atoms and plasmonic nanoparticles. They possess interesting chemical and physical properties [1]. These clusters exhibit fluorescent behavior, where their optical features are size dependent. While usually they tend to aggregate into larger particles, few-atom clusters can be stabilized and protected in solutions using DNA. They do not require great effort in fabrication, but easily self-assemble into DNA encapsulated silver clusters. The dimensions and optical properties of Ag:DNA clusters depend on the DNA sequence. They might prove useful for biological labeling [2] as well as for identifying certain base sequences in genetic studies [3, 4].

We shifted the focus to quantum optical studies on the silver clusters in stead of using the silver clusters to investigate DNA. To study the feasability of the use of these intriguing fluorophores for quantum optical studies, they can be positioned on DNA scaffolds. Here also no complex fabrication is needed, since the DNA scaffolds self-assemble out of single DNA strands and they can be programmed to self assemble with silver clusters on them. In fact, the size selectivity, ease of creation and positioning of these optical emitters could potentially rival quantum dots in their suitability for certain optical coupling studies.

In this thesis, we take an important first step in positioning silver clusters on a DNA scaffold and characterizing their fundamental properties. We use DNA nanotubes as a scaffold and describe features of DNA tubes with different kinds and concentrations of silver clusters. We explore spectral and photostatistical properties of the DNA encapsulated silver clusters on the scaffold at room temperature and at low temperatures. We start by investigating optical and other properties of DNA tubes more closely and find a tendency of tubes to tangle together in smaller or larger structures, depending on different factors. We continue by taking a closer look at the spectral features of our tubes at room temperature and at low temperatures and comparing the results with the spectral features of silver clusters without the tubes. Finally, we initiate photon statistics experiments in a first step to directly observing quantum optical coupling on DNA-templated fluorescent silver nanoclusters.

2 Theory

2.1 DNA encapsulated silver clusters

Showing molecule like fluorescent behavior, silver clusters take an interesting position between single silver atoms, nanoparticles and eventually the bulk silver metal. Due to aggregation, silver nanoclusters are usually not stable in aqueous solution, but they can be size-stabilized by encapsulating them with DNA. The silver clusters form a fluorescent species of which the optical properties are size and DNA sequence dependent [5]. Ag clusters form on single stranded DNA, e.g. oligomers formed like hairpins can be used as hosts for the silver (see Figure 1). The hairpins consist of a single stranded loop where the silver cluster forms and a double stranded stem which could be positioned on a DNA scaffold. Photophysical properties of the fluorescent species of DNA loops with silver clusters have been characterized. The spectral characteristics of the Ag:DNA can be tuned by selecting the base sequence and secondary structure of the DNA strands. Loops with many C or G bases provide the best results [6].

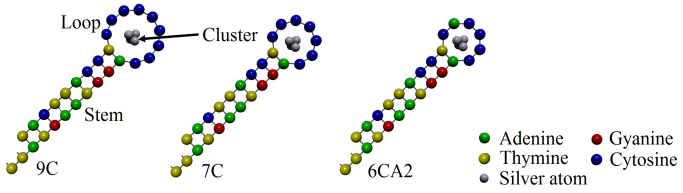

Figure 1: Cartoons of DNA oligomers formed like 9C, 7C and 6CA2 hairpins with silver clusters. The hairpin consists of a double stranded DNA stem and a single stranded DNA loop with a silver cluster in it. The stems of the different hairpins are the same, but the loops differ in the number of cytosine bases. 6CA2 has an adenine base in stead of one of its cytosine bases.

O'Neill expanded the hairpin studies by investigating loops, only consisting of cytosine bases [7, 8]. The spectra of this fluorescent species contained both red and green peaks, the wavelengths and intensities of which varied with the number of cytosine bases in the loop. Specific DNA sequences typically showed coupling between the decay of the red peak and the rise in the green peak, suggesting two fluorescent species linked by some chemical reaction. The guest silver formed clusters typically consisting of around 10 atoms. Absorption and emission wavelengths depend critically on the number of silver atoms in a cluster.

In order to form DNA encapsulated Ag clusters, first silver ions interact with single stranded DNA (see Figure 2). When adding a chemical reducing agent like $NaBH_4$, the silver ions become atoms and cluster together on the DNA. In this way DNA encapsulated silver clusters form [9].

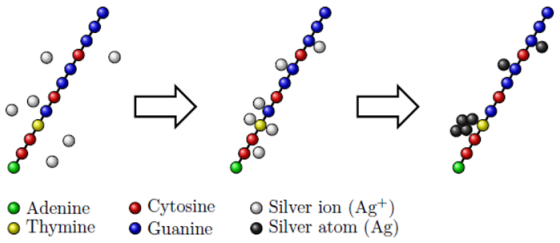

Figure 2: Cartoon of silver atoms forming DNA encapsulated silver clusters by reduction. First silver ions interact with the single stranded DNA. When adding a chemical reducing agent, the silver ions become atoms and tend to cluster together on the DNA strand [9].

2.2 Fluorescence

As stated before, few-atom silver clusters stabilized by DNA produce visible fluorescence. After a molecule has absorbed electromagnetic radiation and an electron is excited to a higher electronic level, it can decay via phosphorescence, fluorescence and non-radiative decay processes. When the electron decays to the ground state via the triplet state, it is called phosphorescence. When it decays from a singlet state to the ground state directly, it is called fluorescence. Aside from electronic levels, particles have all kinds of energy loss mechanisms, such as vibrations, rotations and perhaps electron electron scattering [10, 11]. Absorption and fluorescence can occur from any set of energy levels in ground and final state, so with (relatively) large and complicated DNA molecules there are many possibilities [12].

Besides radiative processes, where a molecule emits or absorbs a photon, non-radiative processes also occur. Consequently, if a molecule is not completely isolated from its surroundings, which is mostly not the case, the fluorescence will not be resonant. Due to non-radiative decay processes the electron will decay to some lower vibrational level and then decay to a lower electronic level and emit a photon with a lower energy than the absorbed photon. Therefore the emitted fluorescence light will be redder than the excitation light [12].

There are various things which may influence fluorescence spectra. Important are the surroundings: if a molecule is surrounded by many other molecules, for instance in a fluid at room temperature, it will have vibronic and electronic interactions with the solvent and solute. Due to those non-radiative interactions there will be various possible levels for the electron to move to and from and the spectrum will be very broad [12] (see Figure 3). When cooling down, several of these interactions may disappear, resulting in a more narrow spectrum at low temperatures.

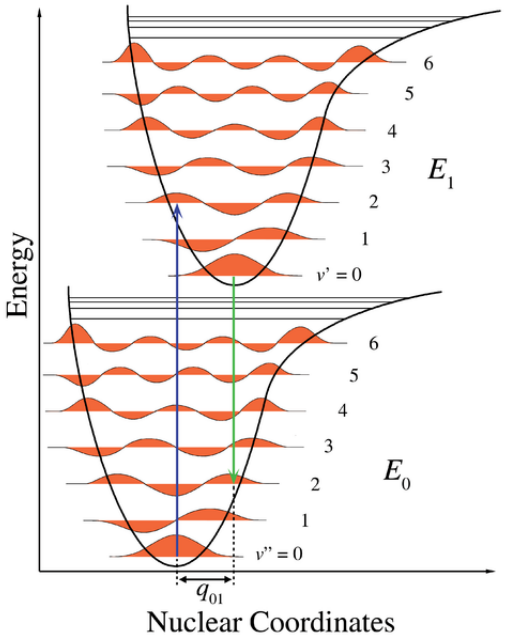

Figure 3: The potential energy curves of a molecule or silver cluster in the electronic ground state and in a higher state, both showing vibrational levels as well as electronic. The more the two curves overlap, the more efficient the molecule is excited and the more intense the emitted light is. The blue arrow indicates absorption, the green arrow indicates fluorescence and the difference between the arrows indicates non-radiative decay paths [http://commons.wikimedia.org/wiki/File:Franck-Condon-diagram.png].

2.3 Single molecule spectroscopy

Experiments observing ensembles of molecules over a period of time can provide some information about their optical characteristics. While the large number of molecules yields a good signal quality, it results in an averaging over the individual spectral features and therefore a sum of statistical distributions and temporal fluctuations. In contrast, single molecule fluorescence spectroscopy provides information about the emission and absorption behavior of an individual molecule. It dispenses new insights about the coupling of single molecules to local environments [13].

Optical experiments on single molecules started with single atoms and ions in gas phase. Single molecules in condensed matter were much more difficult to detect, because of the emission of the surrounding background and the limitation of photobleaching of the single molecules [14].

Bleaching means that due to a chemical reaction a molecule changes and does not show fluorescence any more. This differs from blinking, where the molecule does not fluoresce for a small amount of time. Blinking can appear because the electron goes to some longer living dark state or the molecule undergoes some reversible chemical reaction [14].

In 1989 a single molecule was first detected optically by means of absorption [15]. The year later it was shown that fluorescent single molecule spectroscopy is easier and gives much narrower lines than the absorption method [16].

Although using the same methods as for single molecule spectroscopy, we have not been looking at exactly single molecules, but observed a few emitters.

2.4 DNA tubes

DNA strands can self-assemble in a variety of shapes such as squares, circles, cubes, spheres and tubes [17]. DNA structures can be made using DNA tiles [18]. Additionally, DNA can be programmed to form arbitrairy patterns, e.g. stars and smileys, on a DNA scaffold. This is called scaffolded DNA origami [19]. We decided to use a relatively simple approach for our sample, patterning DNA hairpins using a DNA nanotube as a scaffold.

We make tubes, using DNA tiles consisting of five DNA strands that form a rectangular core with loose ends as designed by Winfree and Rothemund and adjusted by O'Neill [7]. The rectangle of the tile consists of two double helices that cross over to each other at two different places. In Figure 4 the yellow and red strand start as a double helix, but at a certain point, the yellow one crosses over and combines to a double helix with the green strand. The red one combines to a double helix with the blue strand. This twining of strands results in the formation of a DNA tile. The unpaired parts of the DNA, called sticky ends (yellow and purple in Figure 4) are hanging loosely on two sides of the tile and can combine with each other. If they do so, a lattice of tiles is formed [7]. Due to the helicity of the strands these particular tiles do not form a flat lattice, but combine at an angle with respect to each other, thus assembling into tubes [20]. To form the DNA tubes reliably by annealing, the melting temperature of

the tubes should be higher than that of the tiles, so the single stranded DNA can first form tiles and those tiles can combine into tubes [17].

2.4.1 DNA tubes with silver clusters

One of the DNA strands in the tiles of the tubes can be modified to include a hairpin [20]. Silver clusters in hairpins on DNA tubes were stabilizied by O'Neill (see Figure 5), who estimated a chemical yield of 45%. As he found the tendency of tubes to tangle with each other, he suggested that Ag^+ ions mediate the formation of tangles from initially separate tubes [7].

2.4.2 Quantum optics on DNA tubes

It has been shown that the silver clusters behave like atoms or molecules in the sense of having discrete energy levels [1]. To study the feasability of silver clusters as quantum emitters, we need to be able to position them precisely with respect to each other. DNA tubes with hairpins and silver clusters could be suitable for doing quantum optics experiments on them [1]. Comparing the optical properties of silver clusters in hairpins with silver clusters on a tube can indicate quantum coupling. It would also be interesting to see the difference between the photon statistics of a single silver cluster and one that is on the tube. Namely, it may be possible to see the transition from antibunching to bunching (see Section 2.5.2).

2.5 Photon statistics

Quantum optics studies the consequences of considering a beam of light as a stream of photons instead of a classical wave. The differences between the two approaches are rather subtle. In photon counting experiments it is important to distinguish between effects caused by the statistical nature of the photon detection process and the photon statistics of the light beam. Various effects can be explained by treating the light classically and the photoelectric effect in the detector quantum mechanically. A photon detector works like a Geiger-Muller counter: if a light beam falls on the detector, it produces short voltage pulses which the counter registers [21]. Photon statistics betrays something about the quantum mechanical behavior of an emitter.

2.5.1 Correlation functions

The intensity fluctuations of a light beam can be described by a second order correlation function (the first order correlation function is of the electric field, the second order correlation function describes the intensity). The function is defined as follows:

$$g^{(2)}(\tau) = \frac{\langle I(t)I(t+\tau)\rangle}{\langle I(t)\rangle\langle I(t+\tau)\rangle}, \tag{1}$$

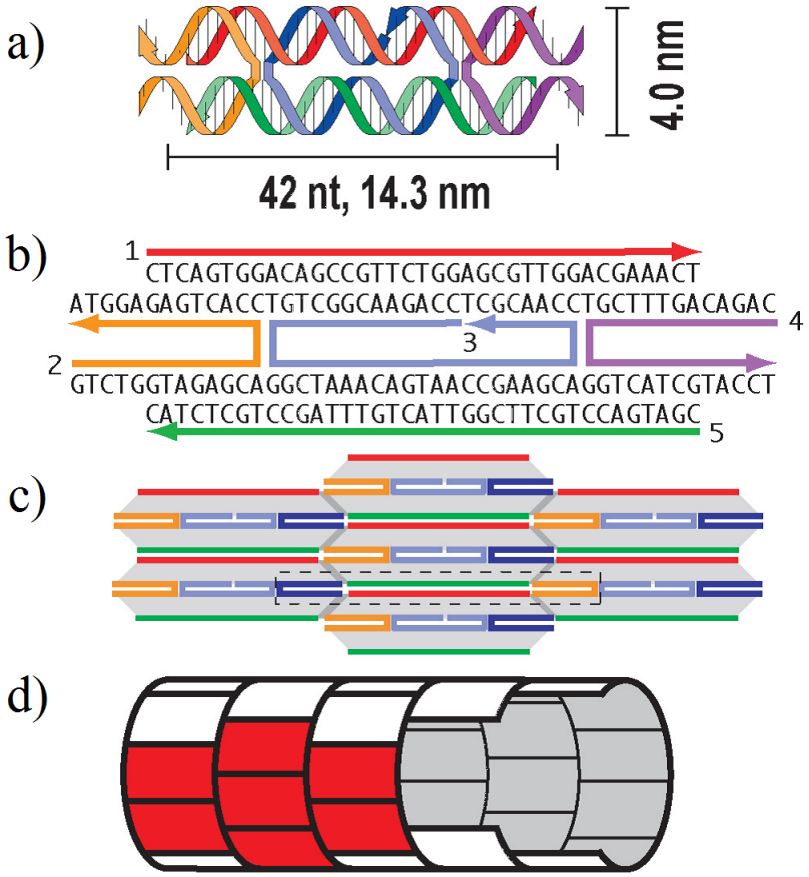

Figure 4: DNA tiles consisting of five strands that form a rectangular core with loose ends. The core consists of two double helices that cross over at two different places (the yellow with the blue strand and the blue with the purple strand). The unpaired parts (yellow and purple) that are called sticky ends are hanging loosely on two sides of the tile. They tend to combine with each other forming a DNA tube [7].

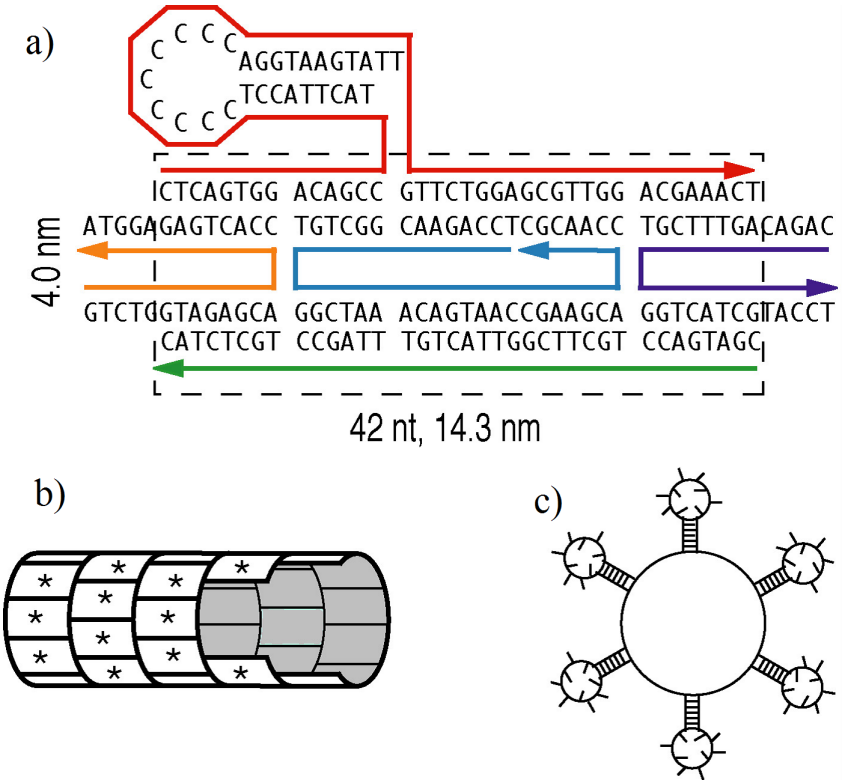

Figure 5: DNA tile consisting of five strands that form a core with loose ends and a hairpin on it. The tiles tend to combine with each other forming a tube with hairpins sticking out of it [7].

where $\langle\rangle$ indicates the time average. In this function the intensity is delayed by τ and multiplied by itself and the product is plotted as a function of the delay [14].

2.5.2 Bunching and antibunching

Light can be classified based on the second order correlation function into bunched, coherent and antibunched light. In the first class $g^{(2)}(\tau) > 1$ and photons are clumped into bunches; this is the case for thermal light.

The photons in a coherent light beam are chaotically ordered, so the time intervals between two photons are random. $g^{(2)}(\tau) = 1$, because the delayed function is perfectly coherent with the function itself.

The last class where $g^{(2)}(\tau) < 1$, has a purely quantum nature. Between the photons in an antibunched beam there are regular gaps.

Emitters in an ensemble are typically statistically independent, so they will all emit at different times. Therefore antibunching effects can only be studied counting photons of exactly one emitter, otherwise it will not be clear what photon belongs to what emitter [21]. Measuring the photon statistics of coupled emitters will give bunching effects [22].

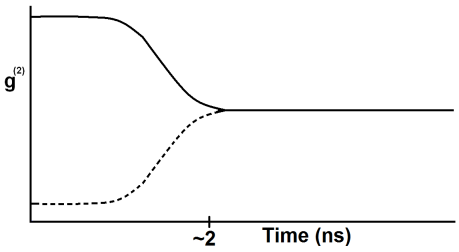

Figure 6: Cartoon of bunching (solid line) and antibunching (dashed line) effects. The timescale on which the effects can be seen for our emitters, is tens of ns.

2.5.3 Experiment

If ideal detectors would exist, the easiest way to detect the correlation function would be to take some single emitter and record the photons that it emits as a function of time [14]. Unfortunately, since detectors cannot count more than one photon at the time but need some time to recover after a photon count, and since they always have internal noise, detectors are not perfect [21].

Recovery time problems can be circumvented and $g^{(2)}(\tau)$ can be measured by using a Hanbury Brown and Twiss setup. In this configuration, the beam is split in two and the coincidence between the photons is measured by using two detectors. In this way the cross correlation between the beams that fell on the first and the second detector are measured. The most practical way of measuring

quantummechanical effects is actually doing a start-stop experiment: to measure the time between the first photon arriving in one detector and the next one arriving in the other detector. If $C(\tau)$ is the probability of measuring the next photon at time τ if you measured one at time 0, and $\mathcal{P}(\tau)$ the probability of measuring any photon at time τ if you measured one at time 0, they are related in this way:

$$\mathcal{P}(\tau) = C(\tau) + \int_0^\tau C(\tau - t_1)C(t_1)dt_1 + \int_0^\tau dt_1 C(\tau - t_1) \int_0^\tau dt_2 C(\tau - t_2)C(t_2) + ... \tag{2}$$

$\mathcal{P}(\tau)$ is also related to $g^{(2)}(\tau)$,

$$\mathcal{P}(\tau) = \langle I(t) \rangle g^{(2)}(\tau). \tag{3}$$

This means long correlation times cannot be measured with start-stop experiments, but those experiments are well suited for measuring short correlations like antibunching [14].

3 Experimental methods

3.1 Samples

We studied various DNA tubes with 9C hairpins, 6CA2 hairpins and 7C hairpins (see Figure 1), using the recipe established previously [7] (see Section A.2 1 for the recipes). As explained before (see Figure 5), we let tiles and tubes anneal from five different DNA strands. We put the PCR tubes containing our sample in a thermos with hot (90 °C) water and allowed it to cool down over a period of two days to room temperature. After that, we synthesized Ag clusters on the hairpins on the tubes. Aside from tubes where all the tiles contained a hairpin, we also made tubes where 50% or 75% of the tiles were substituted by tiles without hairpins. Due to the self-assembly process, the different tiles were randomly distributed over the tubes. For comparison, we also studied single 9C hairpins (not attached to tubes) with silver clusters.

3.2 Fluorimetry

To verify that the DNA tubes fluoresced and to find an indication of their spectral features, we performed fluorimetry, which means characterizing the tubes and hairpins in the visible regime (emission and excitation wavelength 400nm-800nm) (see Section A.3 for specifications of the fluorimeter).

3.3 Microscopy

Using a fluorescence microscope with an oil immersion objective, the samples could be visually inspected to confirm the existence of fluorescent tubes. To this end, we prepared our sample by adding polyvinylalcohol(PVA) to the annealed tubes. Subsequently, we spin coated the sample on a thoroughly cleaned coverslip or substrate. In this way the water was blown off and the DNA and PVA formed a thin film on the coverslip or substrate, immobilizing the DNA tubes. To verify that the tubes were actually formed, we made DNA tubes without hairpins, but with a fluorescent label, 6-carboxyfluorescein (FAM). After that, we inspected the tubes with 9C, 6CA2 and 7C hairpins with silver clusters on them.

3.4 Setup

Our setup was built to i) make images of the sample ii) take spectra of emitters iii) count photons (see Figure 7) (see Section A.4 for specifications). Measurements could be performed at room temperature as well as at low temperatures.

In the excitation path we used a dye laser which could be tuned at wavelengths from 575nm to 595nm (see Figure 7 for a cartoon of our setup). We held the laser power constant with an electro-optic amplitude modulator with feedback loop and used several filters to remove unwanted stray light. We used neutral density filters to set the desired laser intensity.

The sample was mounted in a cryostat which we could cool down to cryogenic temperatures. To avoid condensation on the windows during cooling, we purged the helium vat with helium gas. In order to cool the sample down to temperatures around 220K, we filled the nitrogen jacket with liquid nitrogen (see Figure 7 for a sketch of the cryostat). Adding liquid helium the temperature dropped to 4K. To cool down further to 1,7K, we pumped on the helium vat causing the liquid helium to become superfluid. Because of the absence of bubbles in the superfluid helium, the sample could be imaged nicely.

In the collection path we again used filters to remove unwanted laser light and see only light emitted from the sample. When taking images of the sample, we used a wide field lens to illuminate a larger field of view on our sample (50-100μm) and set the laser intensity to 5mW. Images were recorded with a CCD camera with a magnification of 120 times and using an integration time of 10s at a wavelength of 575nm, 580nm, 585nm, 590nm and 595nm.

Before taking spectra of single emitters, the wide field lens was removed so that our laser beam had a waist of 975nm on the sample. Subsequently, we located several emitters based on the image taken previously at 585nm. The emitters were then selected by using a fast steering mirror. Spectra were taken using an integration time of 60s, a laser intensity of 0,5mW and at the same wavelengths as with the images (from 575–595nm with 5nm increment). Besides spectra of single emitters, spectra of a wider field of our sample were taken by using the wide field lens and a laser intensity of 5mW.

In both cases, taking spectra of single emitters or of a wide field, the signal was relativily weak. To improve the signal to background ratio, we therefore subtracted the background from the emitter signal. To use as a background, we either took spectra of a piece of dark foil or of a position without emitters on our sample. When taking spectra using the wide field lens, we used the spectra of the piece of dark foil as a background. Because of the high concentration of emitters, for the spectra of tubes that was the best background as well. For the spectra of single hairpins it did not really matter what background we used, so we used both and compared the results.

Finally, time traces and start stop measurements were recorded. We took time traces of emitters on our sample using one photon detector and tried to do start stop experiments using two photon detectors.

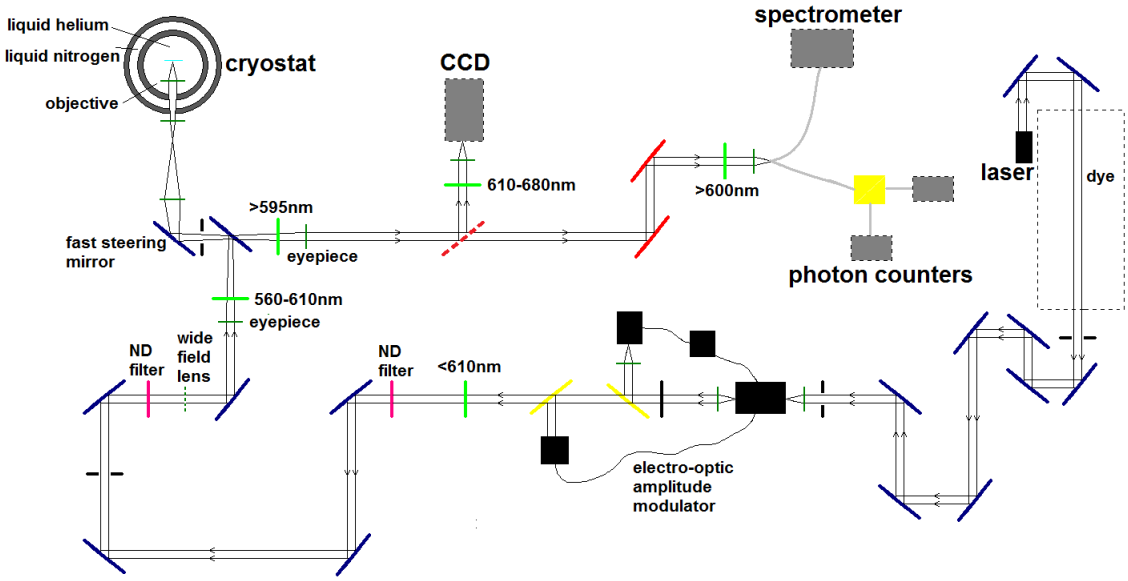

Figure 7: Excitation path: light of the dye laser is modulated by the electro-optic amplitude modulator, then goes through filters and if necessary the wide field lens and is collected on the sample in the cryostat by the eyepiece, the fast steering mirror and the objective. Collection path: light of the sample is collected by the objective, fast steering mirror and the eyepiece and detected by the CCD camera, the spectrometer or the photon counters.

4 DNA tubes

4.1 Results

4.1.1 Fluorimetry

The spectral properties of our of ensembles of 9C, 7C and 6CA2 tubes and 9C hairpins were first characterized with fluorimetry (see Section A.2 for the used concentrations).

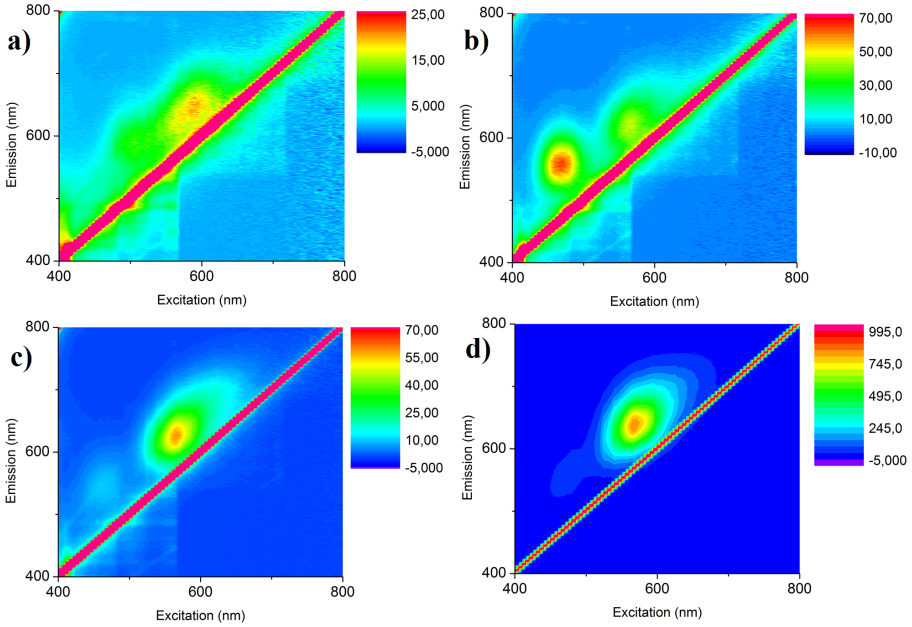

Figure 8: a) Fluorimetry on 6CA2 tubes. The red excitation peak is at 565nm, the emission peak is at 627nm. b) Fluorimetry on 7C tubes. The red excitation peak is at 565nm, the emission peak is at 627nm. c) Fluorimetry on 9C tubes. The red excitation peak is at 565nm, the emission peak is at 629nm. d) Fluorimetry on 9C hairpins. The red excitation peak is at 565nm, the emission peak is at 638nm. The difference in intensity between the 9C tubes and hairpins is caused by a difference in concentration (see Section A.2 for the final concentrations).

As with fluorescent Ag:DNA reported before [7, 8], these spectra show a red and a green species of fluorescent DNA. We are especially interested in the red peak, as this is the species that we can excite with our laser. The peaks of the tubes with different hairpins vary [5, 6, 8] (see Figure 8a,b,c). The red peaks of the 9C tubes and the 9C hairpins fluorimetry are approximately at the same wavelengths (see Figure 8c,d). Note the difference in scale: the 6CA2 tubes are dimmer than the 9C and 7C tubes. The difference in intensity of the 9C

tubes and hairpins is caused by a difference of 25 times in concentration (see Section A.2 for the final concentrations).

4.1.2 Microscopy

To verify that our annealing process (see Section 3.1) yielded DNA tubes, we started by assembling FAM tubes. Figure 9 shows that tubes of approximately 10μm long were formed succesfully. They are well visible and evenly spread over the coverslip.

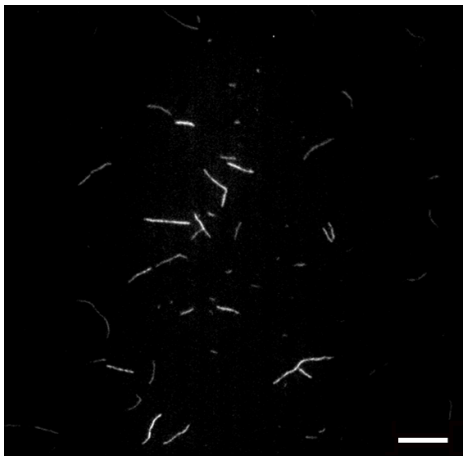

Figure 9: FAM labeled DNA tubes under the microscope; the scale bar is 10μm.

4.1.3 9C tubes

We proceeded by making 9C tubes with DNA encapsulated silver clusters (see Figure 10), which clustered into tangles. We found that the size and distribution of the tangles depends on the concentration of DNA and PVA used. If a thicker PVA or a higher concentration of DNA is used, the tangles are larger and easier to find (see Section C for an overview and pictures).

Figure 10 shows two pictures of the same tangle, but excited at different wavelengths. As stated before (see Section 4.1.1), two different types of clusters are formed which emit at different wavelengths. Figure 10 shows that the red and the green emitters are both uniformly distributed on the tangle. The tangles are coloured red and green using software, according to what we had observed.

Additionally, we studied samples with the same concentration of DNA, but with less hairpins and silver (see Section 3.1 and Section A.2). Figure 11 shows that the tubes had smaller tangles and were less bright than the 9C tubes where all the tiles contained a hairpin.

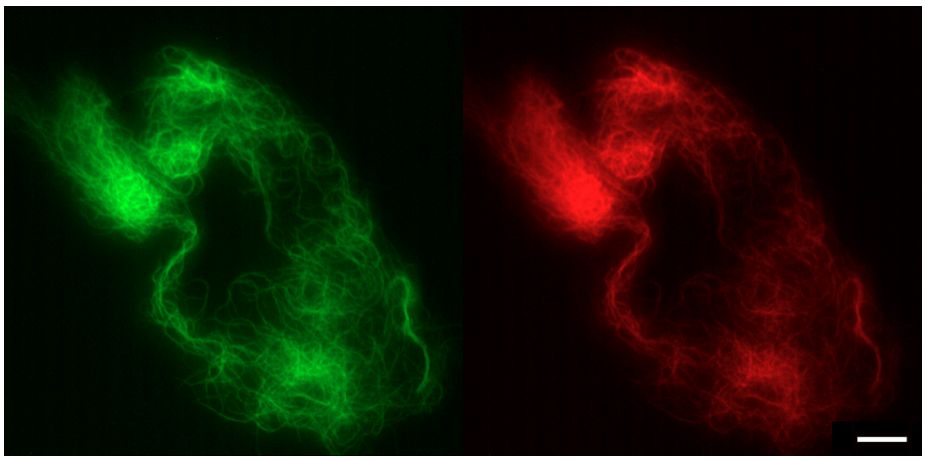

Figure 10: 9C tubes under the microscope. We took pictures of the green (left) and red (right) emitters on the same tangle using blue and green excitation respectively; the scale bar is 10μm.

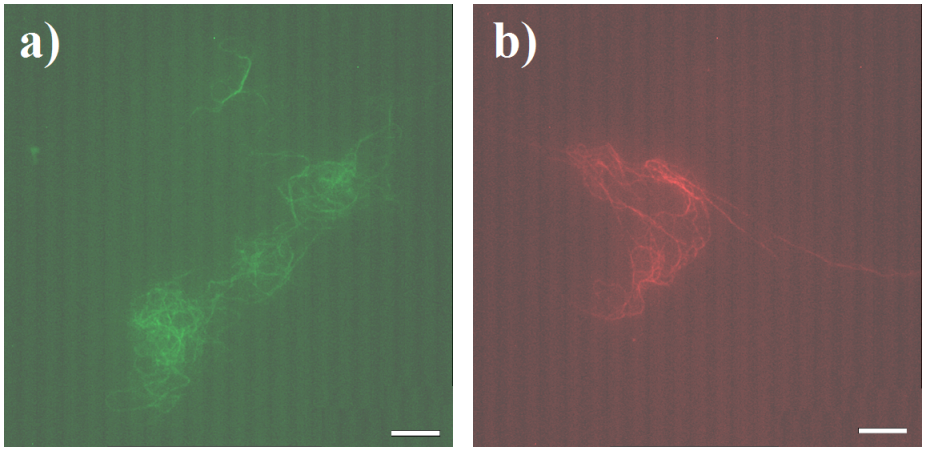

Figure 11: a) 9C tubes under the microscope with 50% hairpins. b) 9C tubes under the microscope with 25% hairpins. The intensity of these tubes is lower and they are less compactly tangled than the tubes with 100% hairpins; the scale bar is 10μm.

4.1.4 Tubes with other hairpins

There is also a difference between the tangles formed by tubes with other hairpins on them. 7C tubes for instance seem to form somewhat looser tangles (see Figure 12, and the tangles of the 6CA2 tubes seem to have a finer structure than those of the 9C tubes (see Figure 13) (see Section C for more pictures).

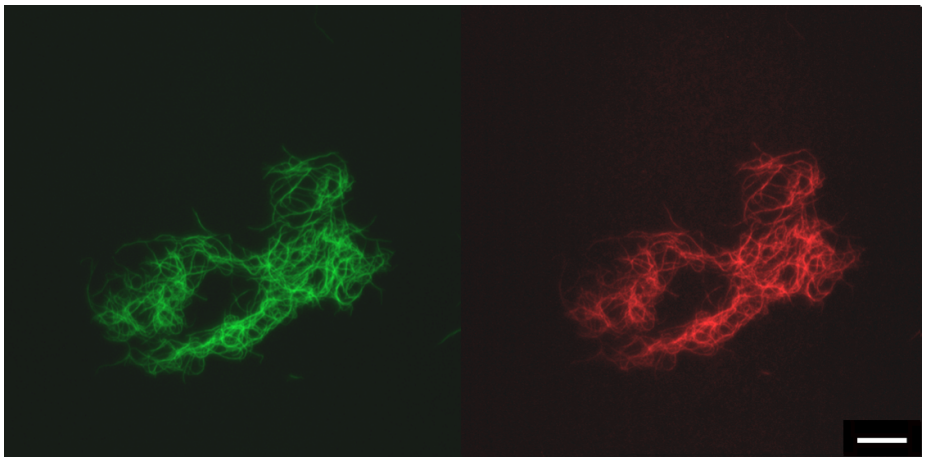

Figure 12: 7C tubes under the microscope. We took pictures of the green (left) and red (right) emitters on the same tangle using blue and green excitation respectively; the scale bar is 10μm.

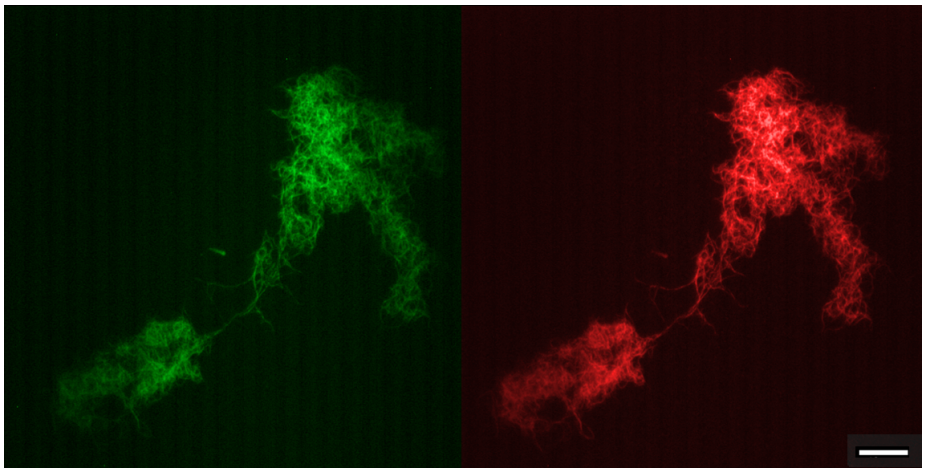

Figure 13: 6CA2 tubes under the microscope. We took pictures of the green (left) and red (right) emitters on the same tangle using blue and green excitation respectively; the scale bar is 10μm.

4.2 Discussion

As alluded to before, the size and distribution of DNA tangles depends on several things (see Section C for an overview). A higher concentration of DNA gives more and larger tangles. A higher amount of hairpins and silver on the tubes results in larger tangles as well (see Figure 11). Our data confirm the suggestion of O'Neill that the silver ions mediate the formation of tangles, because the presence of more silver gives larger tangles.

There is also a relationship between the thickness of the PVA and the distribution and size of the tangles. As could be expected, using a higher concentration of DNA causes the formation of larger and more tangles than with a low concentration of DNA. Interestingly, using thicker PVA gives larger tangles (see Section C for an overview). This is an indication that the environment of the DNA tubes influences the structures.

4.2.1 Tubes with other hairpins

As illustrated by the pictures, the tangles consisting of tubes with different hairpins are not the same. This phenomenon could be caused by a difference in chemical yield; the 9C tubes coudl for instance have much more silver clusters on them than the 6CA2 and 7C tubes and tangle in a different way. Alternatively, it can be that this is not caused by the silver clusters, but is inherent in the tube structure. It could be that the length of tubes with different hairpins varies due to differences in stress. We did not look at differences in chemical yield, but did check the possible difference in tube lengths by looking at the tubes with hairpins, but without silver clusters. These tubes are made visible with an intercalating dye. The result is shown in Figure 14. The 6CA2 tubes with the intercalating dye are smaller than the 9C tubes, so that could explain the finer structure of the 6CA2 silver tangles.

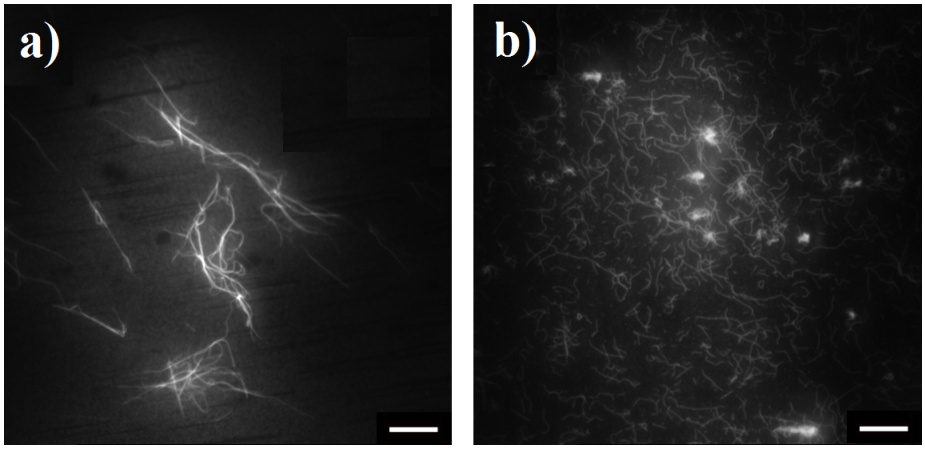

Figure 14: a) 9C tubes without silver but with a fluorescent dye. b) 6CA2 tubes without silver but with a fluorescent dye. The 9C tubes are much longer than the 6CA2 tubes; the scale bar is 10μm.

5 Cryostat

After observing DNA tubes under the microscope, we also looked at the 9C tubes in the cryostat at room temperature, at temperatures around 220K and below 2K (see Figure 15). In the cryostat we had a much smaller translational range than under the microscope, so that is why we used the highest concentration of DNA and PVA (see Section A.2 for recipe) in order to find a tangle in the cryostat. Just as under the microscope, in the cryostat we saw tangles of different sizes and shapes.

The images of tubes and tangles are much sharper under the microscope than in the cryostat. That difference is caused by the fact that the numerical apperture in our setup is lower than under the microscope. Namely, in the microscope we used an oil immersion objective. Because of the similarity in refractive indices of the PVA and the oil, the light that travels through the PVA film to the objective does not refract as much as it does in the cryostat, where there is air between the objective and the sample. Also in our setup we have optical aberrations caused by the cryostat window, so this is why the tubes can be seen much sharper under the microscope than in the cryostat.

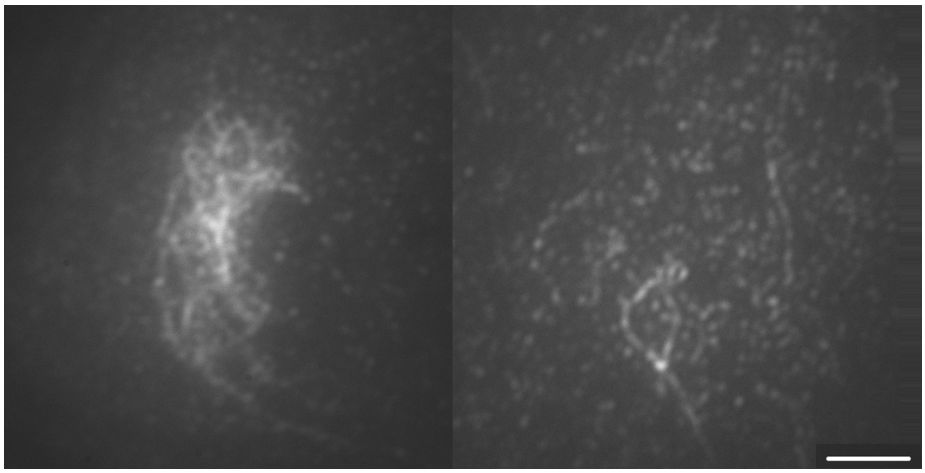

Figure 15: Two typical 9C tangles in the cryostat. Note the presence of loose emitters next to the tangles. The tangles can be seen less sharp in the cryostat than under the microscope. The scale bar is 10μm.

6 Spectral features

6.1 Results

6.1.1 9C tubes spectra at room temperature

First we took some room temperature spectra of emitters at different positions on a sample. We will use the word emitter for a diffraction limited spot on our sample, not to be confused with a single molecule. A so called emitter could be a single hairpin, one tile, a short tube or a bunch of tiles. In Figure 16 the different positions where we took spectra are shown. We took spectra of isolated emittes (A), emitters on crossings of tangles (B) and emitters on tubes (C).

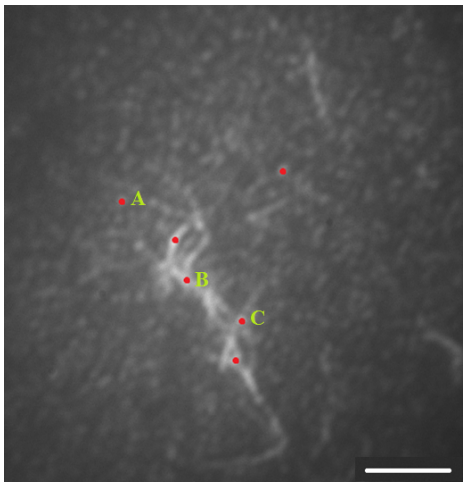

Figure 16: 9C tangle and the positions where we took spectra: on the tangle (B and C) and on isolated emitters (A). Spectra of emitters A, B and C can be found in Figure 17a and Figure 20a; the scale bar is 10μm.

In Figure 17a spectra of emitters on 9C tubes are shown. The spectra of emitters on tubes had three peaks: the first around 618nm, the second around 639nm and the third around 665nm. While changing the excitation wavelength from 575nm to 595nm, the first and second peak became less intense and the third one more intense. So as the excitation wavelength was shifted to the red, so did the emission spectrum of the emitter. The position of the peaks also changed slightly while changing the excitation wavelength.

There were diffferences between spectra of different emitters as well. Some emitters were a lot more intense than others. The shape of the spectrum also depended on the emitter and on the excitation wavelength.

6.1.2 9C tubes spectra at cryogenic temperatures

The spectra at temperatures around 220K and below 2K looked similar to those at room temperature (see Figure 17b,c). They also had three peaks at the same wavelengths as mentioned above, and the third peak was becoming more intense as the excitation wavelength became higher. But there were differences as well. While cooling down, the intensity of the emitters became larger. At temperatures below 2K, the three peaks were less distuinguishable from each other. The spectra at temperatures below 2K were also narrower than those at room temperature; the full width at half maxima were 1,5 times smaller.

It was not possible to reliably find the same emitter at room temperature and at low temperatures. This was caused by the fact that the insert tended to shift when cooling. Additionally, some emitters were very bright at room temperature and blinked or bleached at cryogenic temperatures and vice versa. At best, we can make a statistical comparison.

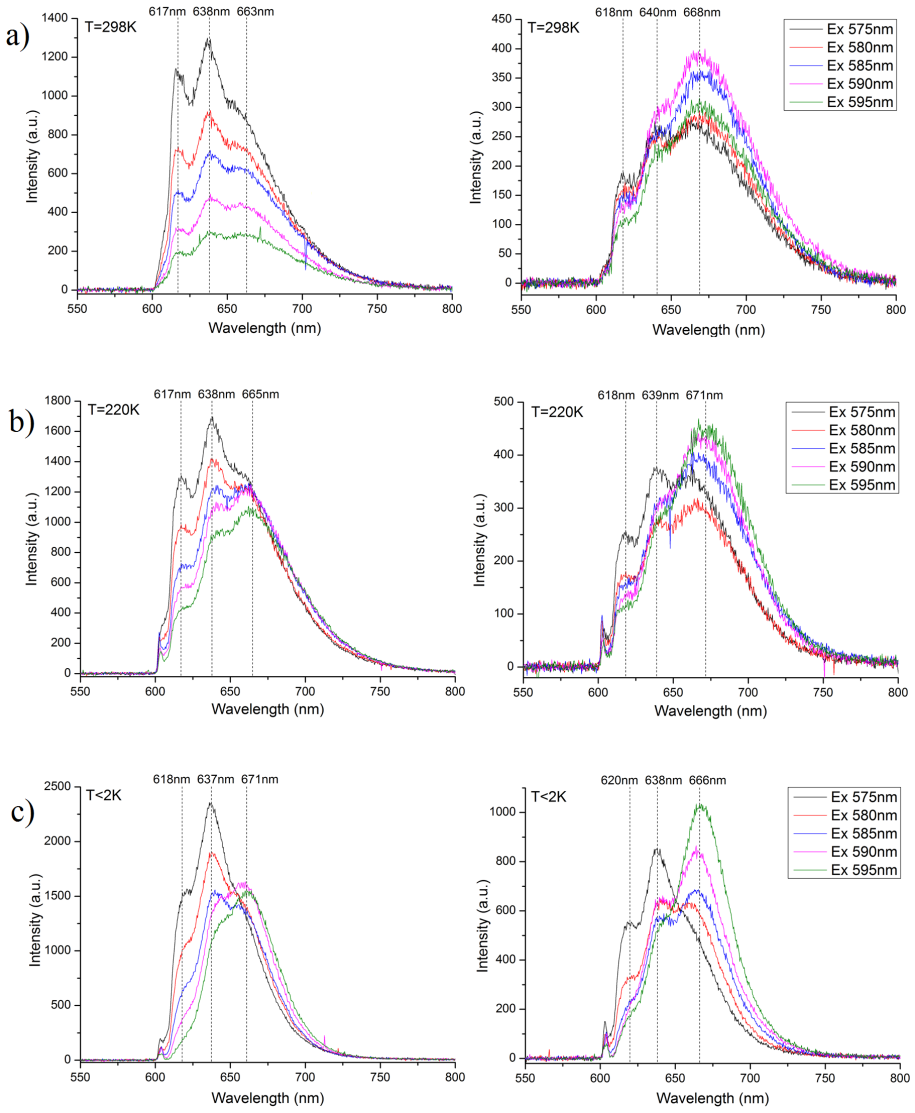

Figure 17: Spectra of two different emitters on a 9C tube, measured at excitation wavelengths of 575–595nm. Note the difference in scale. The left part of the spectra is cut off by filters removing laser light. The dashed lines are put in to guide the eye and show that the three peaks are approximately at the same position. a) Room temperature spectra (the left one is emitter C in Figure 16). b) Spectra at temperatures around the 220K. c) Spectra at temperatures below 2K.

6.1.3 9C hairpins spectra

We also took spectra of emitters in 9C hairpins which had the same strand as the ones on the tubes (see Figure 18 and Figure 19). Interestingly, the room temperature spectra had an on average 15 times lower intensity than those at temperatures around 220K and only 5.5 times lower intensity than those at temperatures below 2K. The spectra looked similar to the spectra of 9C emitters on tubes: three peaks again, shifting to red as the excitation wavelength increased. The difference was the increase in intensity and the 1,5 times narrower peak at temperatures below 2K.

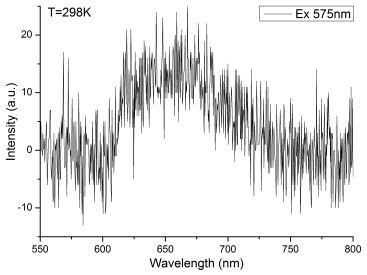

Figure 18: Room temperature spectrum of an emitter in a 9C hairpin at an excitation wavelength of 575nm; spectra at other wavelengths are too noisy to show. The left part of the spectrum is cut off by filters removing laser light.

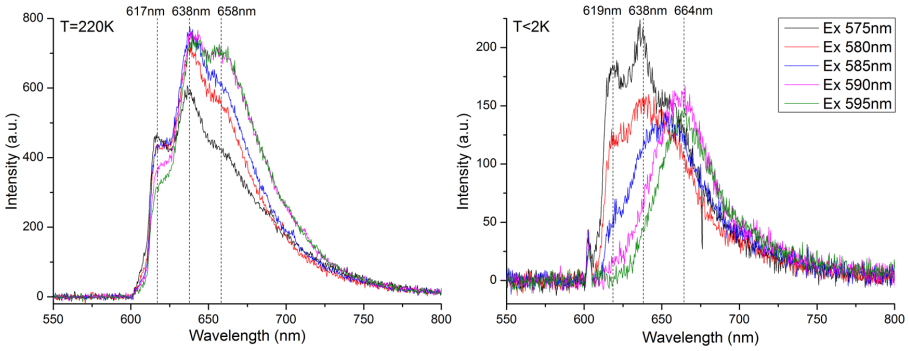

Figure 19: Spectra of an emitter in a 9C hairpin sample, taken at excitation wavelengths of 575–595nm. The left part of the spectra is cut off by filters removing laser light. The dashed lines are put in to guide the eye and show that the three peaks are approximately at the same position. a) Spectrum at temperatures around 220K. b) Spectrum at temperatures below 2K.

6.1.4 Tubes with different silver concentrations

In Figure 20a,b we compare the spectra of emitters on a crossing of a 9C tangle, on a 9C tube, an isolated 9C emitter (called isolated), emitters on a 9C tangle with 50% silver (called 50% tangle), an isolated 9C emitter with 50% silver (called 50% isolated) and two 9C hairpin emitters.

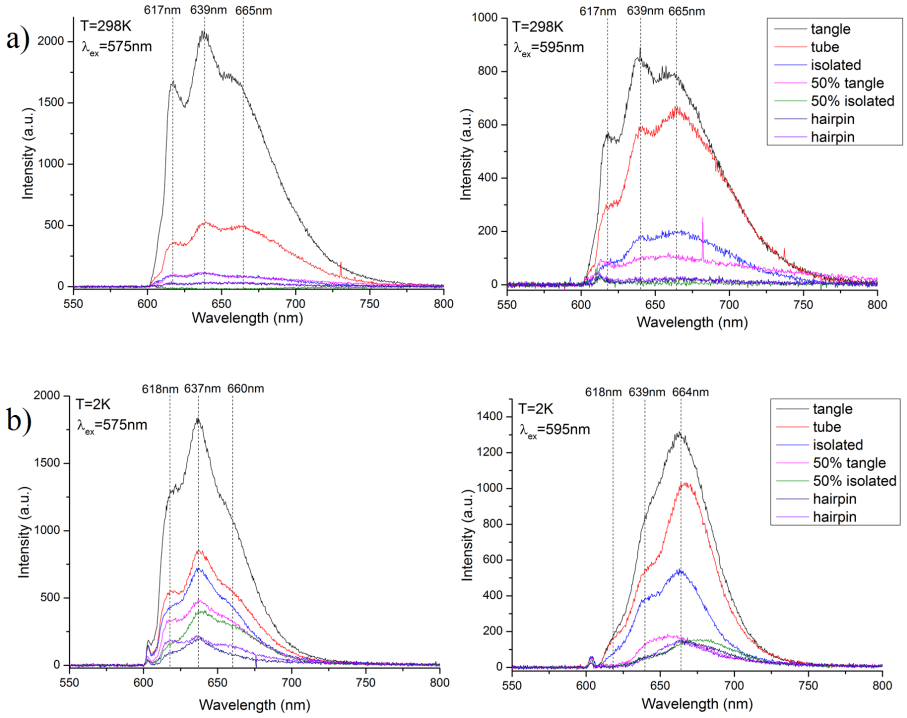

Figure 20: a) Room temperature spectra of different kinds of emitters: 9C emitters on a tangle (emitter B in Figure 16) and on a tube, an isolated 9C emitter (emitter A in Figure 16) a 9C emitter on a tangle with 50% silver, an isolated 9C emitter with 50% silver and two emitters in a 9C hairpins. b) Spectra at temperatures below 2K of different kinds of emitters. The left spectrum is at an excitation wavelength of 575nm, the right one at 595nm. The left part of the spectra is cut off by filters removing laser light. The dashed lines are put in to guide the eye and show that the three peaks are approximately at the same position.

6.1.5 Intensities and linewidths

The largest difference between the various of emitters was their intensity. We compared their intensities by integrating the surface under the spectra (see Table 1 for an overview). We averaged over 10 to 20 positions on a sample.

	hairpin emitters	isolated 50% emitters	isolated emitters	50% tubes	tubes
room temperature	1	0,5	3,7	4,5	19,5
220K	1	no data	0,7	no data	2
2K	1	1,2	2,6	2,6	6

Table 1: Intensities of different kinds of emitters relative to the intensity of the emitters in the hairpins at different temperatures. The intensities increase with larger structures.

At temperatures around 220K, the full width at half maximum is approximately the same as at room temperature. At temperatures below 2K the spectra are approximately 1,5 times narrower.

As stated before, it depends on the kind of emitter how its intensity changes at low temperatures (see Table 2 for an overview). The intensity of hairpin emitters increases at temperatures around 220K and decreases at temperatures below 2K. The intensity of tube emitters and isolated emitters increases at cryogenic temperatures.

	room temperature	220K	2K
hairpin emitters	1	15	5,5
isolated emitters	1	2	2,5
tube emitters	1	2	2

Table 2: Intensities at different temperatures relative to the intensity at room temperature. Note the increase and decrease of the intensity of the emitters in the hairpins. The intensity of tubes also increases at cryogenic temperatures.

6.1.6 7C tubes spectra

Additionally, we took spectra of 7C tubes. Similar to the 9C spectra, the spectra of 7C tubes have three peaks, where the left peak is most visible at 575nm and the right peak at 595nm excitation wavelength. Interesting to notice is that while comparing the intensities of the peaks at an excitation of 575nm and of 595nm, the 7C spectra start brighter and become less bright. That is the case both at room temperatures (see blue and black lines in Figure 21a) and at temperatures below 2K (see black, red and pink lines in Figure 21b).

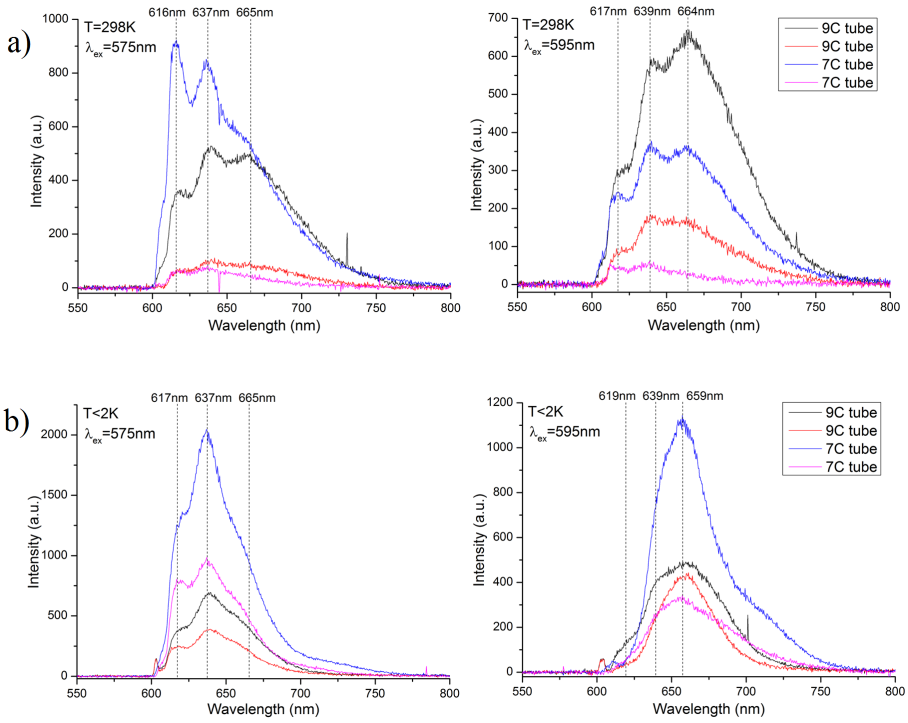

Figure 21: Spectra of two typical 9C and 7C emitters on tubes. At an excitation of 575nm, the 7C spectra are brighter than the 9C spectra, at an excitation of 595nm it is the other way around. The left part of the spectra is cut off by filters removing laser light. The dashed lines are put in to guide the eye and show that the three peaks are approximately at the same position. a) Room temperature spectra. b) Spectra at temperatures below 2K.

6.1.7 Time traces

In previous work time traces of single hairpins gave a good indication that the studied hairpins actually were single molecules. In Figure 22 clear steps down to zero can be distuinguised which indicate that the molecule is blinking on and off. In the present research, we also took time traces of emitters on 9C hairpin emitters (see Figure 23a) and of 9C tube emitters (see Figure 23b). Here it was not possible to distuinguish clear on and off steps down to zero, because we were not able to verify what the background level was. However, multiple levels could be distuinguished indicating multiple molecules.

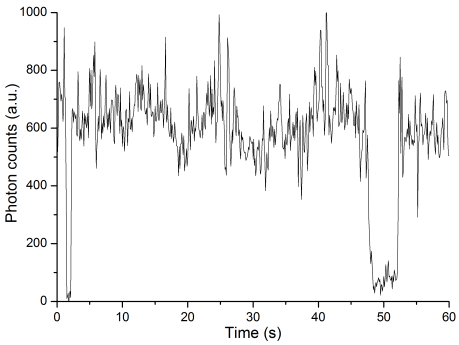

Figure 22: Previous work, time trace of single hairpins. Clear steps down to zero can be seen indicating blinking of the molecule.

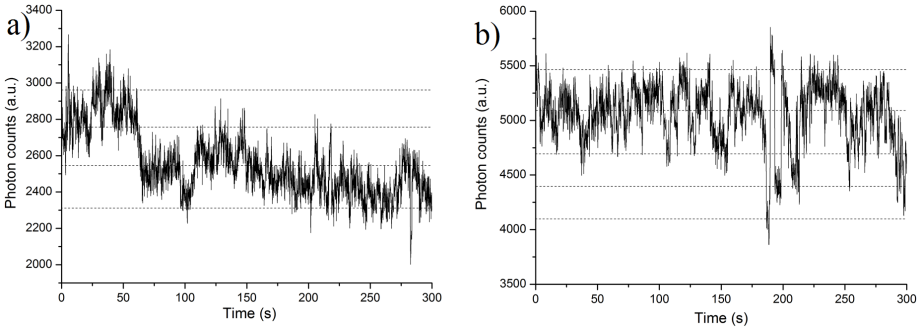

Figure 23: a) Time trace of a 9C emitter in a hairpin. b) Time trace of an emitter on 9C tubes. It is not possible to distuinguish clear on and off steps down to zero because the level of the background was not clear. Possible levels are indicated by the dashed lines.

6.1.8 Photon statistics

As stated before, we tried doing start stop experiments on our emitters with our continuous wave laser to directly observe quantum optical coupling by measuring the transition from antibunching and bunching. When doing photon statistics on DNA tubes, we expected to see bunching and when doing photon statistics on DNA emitters, we expected to see antibunching. This effects should be observable in the first 20ns (see Figure 6). While doing our measurements, most of the counted photons arrive after a delay of 100ns, from which nothing can be concluded about quantum effects (see Figure 24). In the first 100ns we could not see bunching effects due to the many gaps and the low number of counts. The high peak at 32ns is most likely caused by the dead time of the detector,which would mean that one of the detectors was saturated. It would require much more time than the two hours we integrated to collect enough data to see bunching effects. Previous work trying to measure antibunching on single hairpins yielded a similarly sparse histogram, so probably our emitters do not emit enough photons per unit of time. Using a pulsed laser instead of the continuous wave laser could yield better results, because this would give more photons to excite the emitters in the short pulse time of the laser.

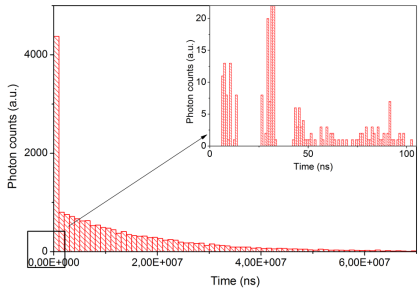

Figure 24: Histogram of a start stop experiment on an emitter on a 9C tube. Most of the counted photons arrive after a delay of 100ns, from which nothing can be concluded about quantum effects. In the first 100ns we could not see bunching effects due to the many gaps and the low amount of photon counts. The peak at 32ns is most likely caused by the detector dead time.

6.2 Discussion

6.2.1 Time traces

Previous time traces of single hairpins clearly show a single step down to zero indicating blinking of a single molecule in one diffraction limited spot (see Figure 22). We took time traces of emitters on 9C tubes and tried to determine how many steps the emitter could blink, before it reached the background level and bleached away (see Figure 23b). In this way information about the number of hairpins on a tube that hold a silver cluster within one diffraction limited spot can be deduced.

The problem is that the level of the background was not clear. As stated before, we either used a black foil or a dark position on our sample as a background for our spectra. But the concentration of emitters in the sample with tubes was so high, that is was not possible to find a real dark position on our sample. We took time traces of the dark foil, but we could not verify whether this really gives the proper background. Taking the background of previous work on time traces of single hairpins, we estimated roughly 12 hairpins in our diffraction limited spot. Even though we could see some steps indicating blinking, we could not estimate the amount of hairpins in one emitter precisely by using time traces.

We also took time traces of 9C hairpin emitters (see Figure 23a). Here the level of the background was not clear as well. The concentration of hairpins in the sample was relatively high, so it was not possible to find a real dark position on our sample. Therefore we could not say much about the precise amount of hairpins we were looking at in our diffraction limited spot, but Figure 23a indicates we were looking at multiple emitters. Taking the background of previous work on time traces of single hairpins again, we estimated eight hairpins in our diffraction limited spot. To have a better estimation, the experiment needs to be repeated with a lower concentration of hairpin emitters.

6.2.2 Three peaks

When comparing the fluorimetry results and the spectra of immobilsed emitters, the difference is the presence of three peaks in the emitter spectra, which the fluorimetry does not show. There are several possible explanations for this difference. We verified whether it could be a contamination, but freshly prepared samples did not yield different results.

Interesting to mention is that the three peaks have not been seen previously in the study of spectra of other single hairpins. The difference between the present and the past experiments are the procedures. While previously the hairpin spectra were obtained using PVA of 5mg/mL and spin coating it for two minutes at 4000rpm, here we used PVA of 50mg/mL and spin coated it for one minute at 2000rpm. The reason we used a different procedure was that we needed a high concentration of DNA and we did not want to disturb our DNA structures by spin coating too fast and long.

The different preparation of samples restults in having a thicker PVA layer which could cause different spectral behavior of the immobilised emitters. A possible explanation is the effect of thin film interference. However, PVA has a refractive index of approximately 1,55 and fused silica which our substrate is made of has a refractive index of 1,46. Neither calculations nor simple experiments with a white lamp shining on our substrate with PVA spin coated on it, indicate the presence of thin film interference strong enough to cause this multipeak phenomenon.

Additionally the fact that we embed our emitters with PVA could cause differences in spectral behavior, compared to fluorimetry. In fluorimetry, 9C and 7C tubes show no difference in excitation peak (see Figure 8b,c). However, immobilised 9C tubes differ in intensity at different excitation wavelengths (see Figure 21). Probably the PVA-immobilized 9C tubes are excited more efficiently at somewhat longer wavelengths than the PVA-immobilized 7C tubes, thus showing different spectral behavior than tubes in solution during fluorimetry.

Yet previous studies of spectra of single hairpins in a lower concentration of PVA mentioned earlier do not show the multipeak behavior which the emitters on tubes and in hairpins do show. It could be that there are some interactions between the guest DNA emitters and the thicker host PVA, which would cause the silver clusters to emit in three different spectral domains and the measured spectrum would be a combination of three Gaussians. The slight changing of the three peaks while changing the excitation wavelength could be caused by this sum of three Gaussians. After all, in a sum of three Gaussians, changing the relative intensities would cause the three peaks in the total spectrum to shift slightly.

Another possible explanation for this phenomenon could be the interaction of multiple emitters close together. It is clear that on the tubes there is a high density of emitters, and time traces indicate that even the emitters of which we thought were single hairpins, were very likely a collection of hairpins (see Figure 23a). On the one hand, the concentration of hairpins in the sample we used could be very high. On the other hand, it is known that higher concentrations of PVA will cause the solution to become more gel-like [23]. This could enable the gathering of many emitters in close proximity, which is why this spectral behavior may also be seen in hairpin samples. Both the interaction between DNA and PVA and the gathering of emitters close to each other could be less present when using thinner PVA. In the future, these possible explanations could be verified by spin coating slower with a PVA of 5mg/mL.

6.2.3 Temperature dependence of intensity

There are some explanations for the observed temperature dependence of the intensity of emitters. As stated before, cooling down will freeze out many rotational and vibrational modes (see Section 2.2). Consequently, the radiative decay paths of emitters can be excited more efficiently when they are colder, so they are brighter. When cooling down to temperatures below 2K, the full width

at half maximum of our emitter spectra becomes 1,5 times as narrow. This is caused by the disappearance of various non-radiative decay channels, resulting in a longer coherence time.

Comparing the intensities of emitters at different temperatures, it is interesting to see their strikingly different behaviour (see Table 1 and Table 2). Hairpin emitters become 15 times as bright when cooled down to temperatures around 220K, but at temperatures below 2K they are only 5 times as bright when compared to room temperature. Presumably this difference is caused by the phenomenon that at temperatures around 220K radiative decay paths become a lot more probable than at room temperature. For unknown reason, at temperatures below 2K radiative decay paths become less efficient, so the emitters are less bright. It could be that at low temperatures, many emitters in close proximity results in quenching, so if there are N times more emitters than in the hairpin sample, the intensity would be $< N$ times as large.

Emitters on tubes are approximately two times brighter when cooled down, which is less than the hairpin emitters. When cooling down hairpin emitters, blinking subsides, which can greatly contribute to their increased brightness at low temperatures. Some silver clusters blink much more frequently than others. Emitters on a tube consist of more silver clusters, so when one cluster blinks frequently, that does not effect the integrated intensity as much as with a hairpin emitter consisting of only a few silver clusters. Probably that is why there is less difference in intensity between a hairpin at room temperature and at cryogenic temperatures and a tube at those temperatures.

6.2.4 Using intensity to determine hairpin amount

Considering the estimated chemical yield of 45% silver clusters on a tube and 7 tiles in circumference of a tube (see Figure 4), and considering the waist of our laser spot to be 975nm, we would expect approximately 430 silver clusters in a diffraction limited spot on a tube. At least if we assume that the silver clusters along the whole circumference of the tube are equally visible, which may not be the case.

Comparing the difference in integrated intensities of emitters on a tube and hairpin emitters could be another way of determining the amount of molecules in one diffraction limited spot on a tube. At room temperature, the difference in intensities between the emitters in the hairpins and the emitters on tubes is approximately 19,5 times, at temperatures around 220K it is approximately 2 times and at temperatures below 2K it is approximately 6 times (see Table 1). Assuming the data at temperatures below 2K the most reliable, because there is less blinking there, we would estimate 6 silver clusters on a diffraction limited spot on a tube.

There are several possible explanations for the difference between 430 and 6 silver clusters in a diffraction limited spot on a tube. Possibly, the data of hairpin emitters and emitters on tubes are just not comparable due to their different temperature dependent behavior. As comparisons of the temperature dependence of the intensity of emitters already indicated, there could be some

form of quenching as well.

It could also be that the chemical yield of 45%, which was found at a very low concentration of hairpins and silver on tubes, is different for the high concentration we used. In this case, silver atoms may tend to gather in larger clusters in the hairpins, resulting in hairpins without silver and hairpins with too much silver fluorescing in a different spectral region.

The estimation of 6 silver clusters in a diffraction limited spot is based on the assumption that we were looking at single hairpins, which however is not a good assumption, because time traces indicate a hairpin emitter consists of more than one molecule (see Figure 23a). This would mean that there are six times as many silver hairpins in a diffraction limited spot on a tube as in a hairpin emitter. Assuming the extimation of 430 hairpins in a diffraction limited spot, the emitters in the hairpin sample would contain tens of molecules. This estimation does not match the previous of eight hairpins on a diffraction limited spot in the hairpin sample and 12 on a diffraction limited spot on a tube. This could be because some of the assumptions we made were not reliable. It is also possible that it indicates a form of coupling between the emitters.

7 Conclusion

In effort to perform quantum optics experiments, we arranged fluorescent silver clusters on scaffolds. We have shown that DNA encapsulated silver clusters can be made and positioned on DNA nanotubes by self-assembly using three different kinds of hairpins. The formed tubes with various hairpins have different lengths. We observed the tendency of the tubes to tangle together. We found that their tangling depends on the amount of silver clusters, the concentration of DNA, their local environment and the DNA sequences of the hairpins.

Studying the DNA tubes at room temperature as well as at low temperatures, the optical properties of the tubes proved to be sequence and temperature dependent. Interestingly, spectra of both emitters on tubes and emitters in the hairpin sample showed three similar peaks. This is likely caused by some interaction between the emitters and their immediate surrounding (polyvinylalcohol) or by the combined emitting of collections of emitters. Possibly this indicates the presence of quantum coupling. We observed that cooling down the emitters changes their spectral properties in such a way that the spectra become more intense and more narrow. The temperature dependence of their intensity was different for emitters on tubes and hairpin emitters, possibly caused by different blinking behavior.

It has not been possible to determine the amount of hairpins in a diffraction limited spot on a tube by using time traces or spectral features. Studies of photon statistics indicate that a different way of measuring is needed.

These results represent an important first step to measuring quantum effects on these intriguing DNA encapsulated silver clusters. Further research should include a better characterization of the factors that influence the DNA tubes and tangles and their optical properties such as the multipeak fluorescence spectra. Future studies of photon statistics using a modulated or pulsed laser beam could provide new insights on quantum optical coupling by observing bunching and antibunching effects.

References

[1] Zheng, J., Dickson, R.M., Nicovich, P.R., *Highly fluorescent noble-metal quantum dots*, 2007, Annual Review of Physical Chemistry, 58, 409–431

[2] Yu, J., Sungmoon, C., Richards, C.I., Antoku, Y., Dickson, R.M., *Live cell surface labeling with fluorescent Ag nanocluster conjugates*, 2008, Photochemistry and Photobiology, 84, 1435–1439

[3] Guo, W., Yuan, J., Dong, Q., Wang, E., *Highly sequence-dependent formation of fluorescent silver nanoclusters in hybridized DNA duplexes for single nucleotide mutation identification*, 2009, Journal of the American Chemical Society, 132, 932–934

[4] Yeh, H.C., Sharma, J., Han, J.J., Martinez, J.S., Werner, J.H., *A DNA-Silver Nanocluster Probe That Fluoresces upon Hybridization*, 2010, Nano Letters, 2010, 10, 3106–3110

[5] Petty, J.T., Zheng, J., Hud, N.V., Dickson, R.M., *DNA templated Ag nanocluster formation*, 2004, American Chemical Society, 126, 5207–5212

[6] Gwinn, E.G., O'Neill, P.R., Guerrero, A.J., Bouwmeester, D., Fygenson, D.K., *Sequence-dependent fluorescence of DNA-hosted silver nanoclusters*, 2008, Advanced materials, 20, 279–283

[7] O'Neill, P.R., *Few-Atom Silver Cluster Fluorophores Stabilized and Arranged at the Nanoscale with DNA*, 2010, PhD thesis, University of California Santa Barbara

[8] O'Neill, P.R., Velazquez, L.R., Dunn, D.G., Gwinn., E.G., Fygenson, D.K., *Hairpins with poly-C loops stabilize four types of fluorescent Ag_n:DNA*, 2009, Physical Chemistry Letters, 113, 4229–4233

[9] Leijssen, R., *Exploring low-temperature optical coherence in DNA-encapsulated silver clusters*, 2010, masterthesis, University of Leiden

[10] Kreibig, U., *Interface-induced dephasing of Mie plasmon polaritons*, 2008, Applied Physics B, 93, 79–89

[11] Weick, G., Molina, R.A., Weinmann, D., Jalabert, R.A. *Lifetime of the first and second collective excitations in metallic nanoparticles*, 2005, Physical Reviews B, 72, 115410

[12] Straughan, B.P., Walker, S., *Spectroscopy 3*, 1976, Chapman and Hall Ltd, London, 161–197

[13] Tamarat, Ph., Maali, A., Lounis, B., Orrit, M., *Ten years of single molecule spectroscopy*, 2000, The journal of Physical Chemistry, 104, 1–16

[14] Orrit, M., *Photon statistics in single molecule experiments*, 2002, Review article Single Molecules, 3, 255–265

[15] Moerner, W.E., Kador, L., *Optical detection and spectroscopy of single molecules in a solid*, 1989, Physical Review Letters, 62, 2535–2538

[16] Orrit, M., Bernard, J., *Single pentacene molecules detected by fluorescence excitation in a p-terphenyl crystal*, 1990, Physical Review Letters, 1990, 65, 2716–2719

[17] Reif, J., Chandran, H., Gopalkrishnan, N., LaBean, T., *Self-assembled DNA nanostructures and DNA devices*, 2010, [online] Available: http://www.cs.duke.edu/∼reif/paper/HandbkNanofabDNA/HandbkNanofabDNA.pdf

[18] Winfree, E., Liu, F.R., Wenzler, L.A., Seeman, N.C., *Design and self-assembly of two-dimensional DNA crystals*, 1998, Nature, 394, 539–544

[19] Rothemund, P.W.K., *Folding DNA to create nanoscale shapes and patterns*, 2006, Nature, 440, 297–302

[20] Rothemund, P.W.K., Ekani-Nkodo, A., Papdakis, N., Kumar, A., Fygenson, D.K., Winfree, E., *Design and characterizaton of programmable DNA nanotubes*, 2004, American Chemical Society, 126, 16344–16352

[21] Fox, M., *Quantum Optics*, 2007, Oxford University Press, New York, 75-123

[22] Raymond Ooi, C.H., Byung-Gyu Kim, Hai-Woong Lee, *Coherent effects on two-photon correlation and directional emission of two two-level atoms*, 2007, Physical Review A, 75, 063801

[23] Liu, M., Cheng, R., Qian, R., *Effect of solution concentration on the gelation of aqueous polyvinyl alcohol solution*, 1995, Journal of Polymer Science B, 33, 1731–1735

A Recipes, procedures and materials

A.1 Strand sequences

DNA strands are ordered at Integrated DNA Technologies. These are the sequences (5' to 3'):

SE1	CTC-AGT-GGA-CAG-CCG-TTC-TGG-AGC-GTT-GGA-CGA-AAC-T
SE1-9C	CTC-AGT-GGA-CAG-CCT-ACT-TAC-CT-CCC-CCC-CCC-A-GGT-AAG-TAT-TGT-TCT-GGA-GCG-TTG-GAC-GAA-ACT
SE1-7C	CTC-AGT-GGA-CAG-CCT-ACT-TAC-CT-CCC-CCC-C-A-GGT-AAG-TAT-TGT-TCT-GGA-GCG-TTG-GAC-GAA-ACT
SE1-6CA2	CTC-AGT-GGA-CAG-CCT-ACT-TAC-CT-CAC-CCC-A-GGT-AAG-TAT-TGT-TCT-GGA-GCG-TTG-GAC-GAA-ACT
SE2	GTC-TGG-TAG-AGC-ACC-ACT-GAG-AGG-TA
SE3	CCA-GAA-CGG-CTG-TGG-CTA-AAC-AGT-AAC-CGA-AGC-ACC-AAC-GCT
SE3-FAM	CCA-GAA-CGG-CTG-TGG-CTA-AAC-AGT-AAC-CGA-AGC-ACC-AAC-GCT/36-FAM
SE4	CAG-ACA-GTT-TCG-TGG-TCA-TCG-TAC-CT
SE5	CGA-TGA-CCT-GCT-TCG-GTT-ACT-GTT-TAG-CCT-GCT-CTA-C

A.2 Recipes

A.2.1 FAM tubes

Final concentrations:

SE1	1,8μM
SE2	1,8μM
SE3-FAM	1,8μM
SE4	1,8μM
SE5	1,8μM
Ammonium acetate	40mM
Magnesium acetate	10mM

A.2.2 9C/7C/6CA2 tubes

Final concentrations:

SE1-9C/7C/6CA2	1,8μM
SE2	1,8μM
SE3-FAM	1,8μM
SE4	1,8μM
SE5	1,8μM
Ammonium acetate	40mM
Magnesium acetate	10mM

A.2.3 9C 50% tubes

Final concentrationsr:

SE1-9C	0,9μM
SE1	0,9μM
SE2	1,8μM
SE3-FAM	1,8μM
SE4	1,8μM
SE5	1,8μM
Ammonium acetate	40mM
Magnesium acetate	10mM

A.2.4 9C 25% tubes

Final concentrations:

SE1-9C	0,45μM
SE1	1,35μM
SE2	1,8μM
SE3-FAM	1,8μM
SE4	1,8μM
SE5	1,8μM
Ammonium acetate	40mM
Magnesium acetate	10mM

A.2.5 9C hairpins

Final concentrations:

9C hairpins	NH_4OAc	$AgNO_3$	$NaBH_4$
50μM	20mM	350μM	100μM

A.2.6 Silver reduction ratios

9C/7C/6CA2 tubes	$AgNO_3$	$NaBH_4$
1,8μM; 50μL	192μM; 2,8μL	1mM; 2,8μL

9C 50% tubes	$AgNO_3$	$NaBH_4$
1,8μM; 50μL	192μM; 2,8μL	1mM; 1,4μL

9C 25% tubes	$AgNO_3$	$NaBH_4$
1,8μM; 50μL	192μM; 2,8μL	1mM; 0,7μL

The DNA solution was combined with $AgNO_3$ and stored at 4 °C for 30 minutes. After that the mixture was reduced with $NaBH_4$ and stored at 4 °C for 12 hours .

A.2.7 Imaging ratios

FAM tubes	PVA
1,8μM; 10μL	5mg/mL; 90μL

9C hairpins	PVA
5μM; 4μL	50mg/mL; 36μL

A.2.8 PVA concentrations

For the imaging of silver tubes we tried several concentrations of DNA and PVA:
10x diluted

DNA tubes	PVA	ammonium acetate/magnesium acetate
10μL	5mg/mL; 80μL	400mM/100mM; 10μL
10μL	10mg/mL; 80μL	400mM/100mM; 10μL
10μL	50mg/mL; 80μL	400mM/100mM; 10μL

5x diluted

DNA tubes	PVA	ammonium acetate/magnesium acetate
10μL	50mg/mL; 35μL	400mM/100mM; 5μL

2x diluted

DNA tubes	PVA	ammonium acetate/magnesium acetate
25μL	50mg/mL; 20μL	400mM/100mM; 5μL

1/3x diluted (highest concentration, also used for samples in the cryostat)

DNA tubes	PVA	ammonium acetate/magnesium acetate
33,3μL	5mg/mL; 11,7μL	400mM/100mM; 5μL
33,3μL	10mg/mL; 11,7μL	400mM/100mM; 5μL
33,3μL	50mg/mL; 11,7μL	400mM/100mM; 5μL

A.2.9 Intercalating dye

DNA tubes	SybrGold dye	ammonium acetate/magnesium acetate	water
1μL	10x; 1μL	400mM/100mM; 1μL	7μL

We dit not use PVA with the intercalating dye samples, but put a drop of 10μL on the microscope slide and put the cover slip on it.

A.3 Procedures

A.3.1 Fluorimetry

Doing fluorimetry on DNA tubes and hairpins, we used the final concentrations mentioned above and did not add PVA.
Fluorescence Spectrophotometer, VARIAN, CARY Eclipse
Excitation: 400nm 800nm
Emission: 400nm 800nm
Excitation slit: 5nm
Emission slit: 5nm

PMT: 800V (high)
Scan Control: Slow or Medium

A.3.2 Spin coating

Microscope: 50μL spin coated for 75s at 2000rpm
Cryostat: 20μL spin coated for 75s at 2000rpm

A.3.3 Filtering

Amicon Ultra Centrifugal filters, MILLIPORE, 0.5mL, 30kD/50kD/100kD

DNA tubes	ammonium acetate/magnesium acetate
50μL	400mM/100mM; 450μL

A.4 Specifications

A.4.1 Setup

579/34 BrightLine Bandpass Filter, 25mm	Laser 2000, Semrock	ff01-579/34-25
593nm BrightLine LWP Edge Filgter, 25mm	Laser 2000, Semrock	ff01-593/LP-25
629/56 BrightLine Bandpass Filter, 25mm	Laser 2000, Semrock	ff01-629/56-25
647/57 BrightLine Bandpass Filter, 25mm	Laser 2000, Semrock	ff01-647/57-25
641/75 BrightLine Bandpass Filter, 25mm	Laser 2000, Semrock	ff01-641/75-25
594 StopLine Notch Filter, U-grade, 25mm	Laser 2000, Semrock	NF01-594U-25
605nm Dichroic Beamsplitter, 25.2 x 35.6 mm	Laser 2000, Semrock	ff605-Di02-25x36
CCD camera	Andor Technology, iKon	CCD-08061
Coherent 899 Ring LASER	Laser Quantum	
Rhodamine CG dye		
Spectrometer	Ocean Optics	QE 65000
Cryostat	Leiden FMD	2343-23 06
Noise eater (Crystal)	Gsanger	LM 0202 AR 632nm
Photon counters	Perkin Elmer	SPCM-AQR-14-FC
Fast steering mirror	Newport	FSM-300 Series
Time tagging card	Cronologic	HPTDC 8-PC1
Mirrors, pinholes, lenses etc	ThorLabs	

To find the focus we used a He:Ne laser and a small CCD camera, connected to a screen.

A.4.2 Microscope

Fluorescence Microscope, Zeiss Axiovert 40 CFL
100x oil immersion objective
Filters:

excitation: 472nm/30nm	dicroic: 495nm	emission: 520nm/50nm
excitation: 530nm/30nm	dicroic:560nm	emission: 600nm/75nm

B Trials

B.1 Filtering

In order to get the concentration of tubes higher and see them with our setup, we tried to filter the solution. For that, we took some DNA and added much buffer. We spinned the filter and a dry PCR tube in a centrifuge for 5 minutes at 14000rpm. After that, we took out the filter with filtered DNA, turned it upside down in a empty PCR tube and spinned it for another 2 minutes at 1000rpm.

After the filtering we did not see tangles any more, so we concluded that the fast spinning broke our structures (see Figure 25).

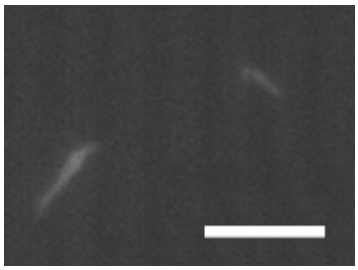

Figure 25: After filtering we did not see 9C tubes tangling any more, we only saw some small tubes; the scale bar is 10μm.

B.2 Self-Assembly

We tried many approaches of putting the sample in the thermos. The sample should have good thermal contact with the water, but the water sould be kept out of the PCR tube to prevent contamination and destruction of the DNA strand by nuclease.

- PCR tube with sample inside a 15mL conical centrifuge tube with a thumbtack in it to make it heavier
    * Disadvantage: there still gets water in the bigger tube
    * The tubes are still not heavy enough, so they float above the water
- PCR tubes with samples inside a 15mL conical centrifuge tube, sealed with parafilm with a screw in it
    * Disadvantage: it is so heavy that it sinks to the bottom of the thermos, where the water is nominally colder
    * The tube is so big that the small tubes do not have good thermal contact with the water

- PCR tube with sample in a floater of foam rubber
    * Disadvantage: floater becomes wet, sinks a little into the water, so that the water can enter the tube
- Bare PCR tube with sample sealed with parafilm
    * The parafilm melts and does not seal properly, so that the water enters the tube and the sample is being destroyed
- PCR tube with sample sealed with parafilm in a floater of foam rubber
    * Disadvantage: floater becomes wet, sinks a little into the water, so that the water can enter the tube
- PCR tube with sample sealed with parafilm in plastic bag within a bigger plastic bag
    * Water comes into the bigger bag
    * The parafilm sticks to the plastic bag: difficult to remove properly
- PCR tube with sample sealed with cling film (Hersluitbare diepvriesza-kken, Jumbo, $-40\,^{\circ}\mathrm{C}$ – $+115\,^{\circ}\mathrm{C}$) in a plastic bag (2-in-1 vershoud- en magnetronfolie, Dumil, $1\,\circ\mathrm{C}$ – $175\,\circ\mathrm{C}$) within a plastic bag
    * Plastic bags melt a little bit: difficult to remove properly

The last approach provides the best results.

C Tangles under the microscope

This is an overview, indicating a relationship between the concentration of DNA and PVA and the tangling of tubes. In the first column information is given about the used tubes and concentrations, the concentrations are explained in Section A.2. In the second column, pictures of two different tangles are shown. Two different types of clusters are formed which emit at either green or red wavelengths and are uniformly distributed on the tangle. The two tangles are colored red and green in software, according to what we had observed. The scale bars are 10μm. The last column describes the observed tangles and indicates the size of the structures. A rough estimation of the distribution of tangles is given in fields of view, where one field of view of the microscope is approximately 100μm.

tubes dilluted with PVA		dimensions and distribution
9C 10x 5mg/mL	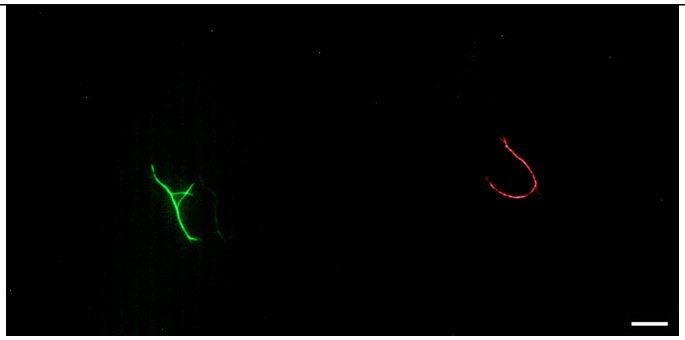	tubes and bifurcations 5-25μm 3 fields of view
9C 10x 10mg/mL	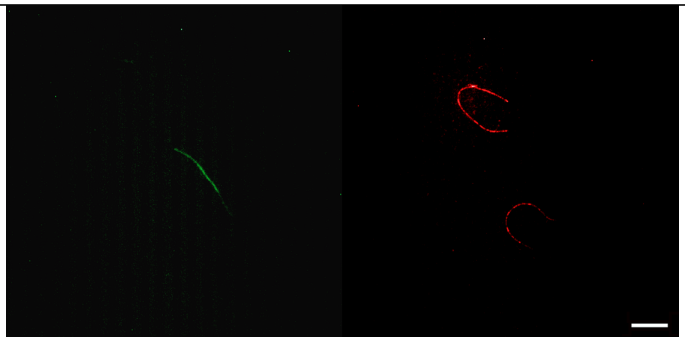	tubes and bifurcations 5-25μm 1,5 fields of view

9C 10x 50mg/mL	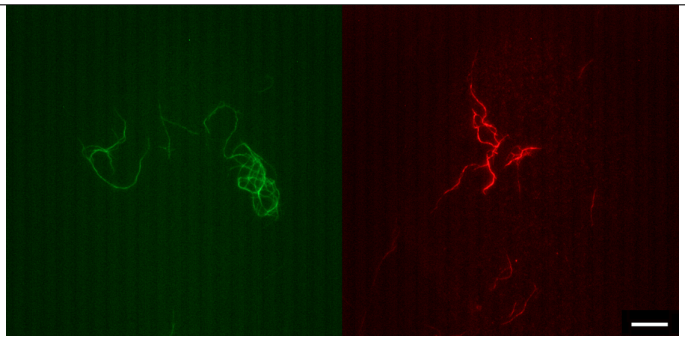	tubes, bifurcations and small tangles 10-40μm 0,5 fields of view
9C 1/3x 10mg/mL	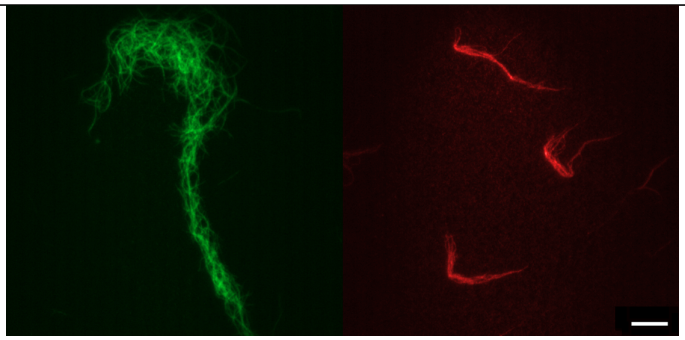	tangles and bifurcations 10-50μm 1 field of view
9C 5x 50mg/mL	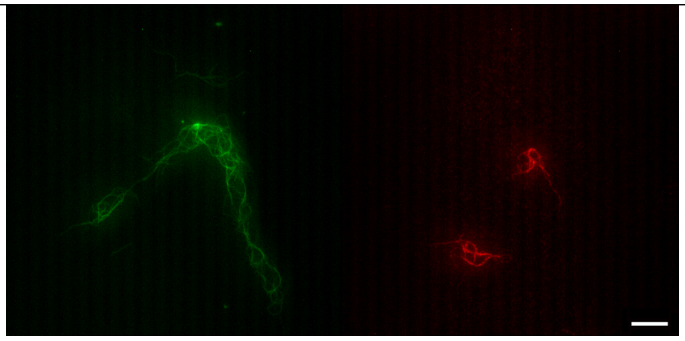	tubes and tangles 10-50μm 2 fields of view
9C 2x 50mg/mL	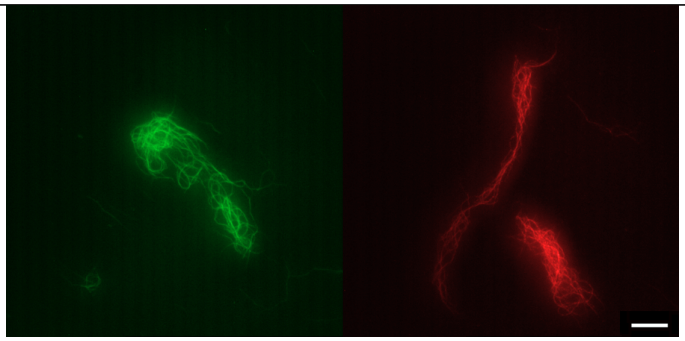	tangles 20-60μm 1 field of view

9C 1/3x 50mg/mL	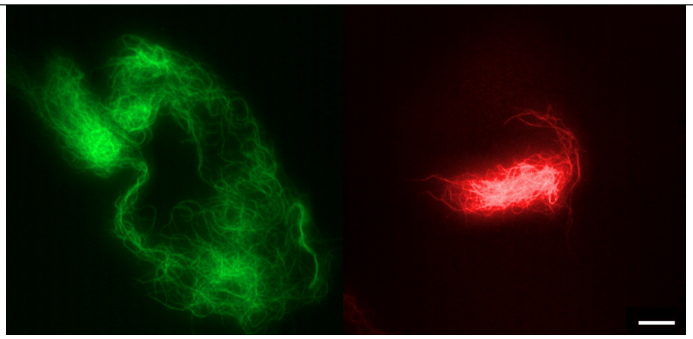	tangles 40-80μm 1 field of view
7C 10x 5mg/mL	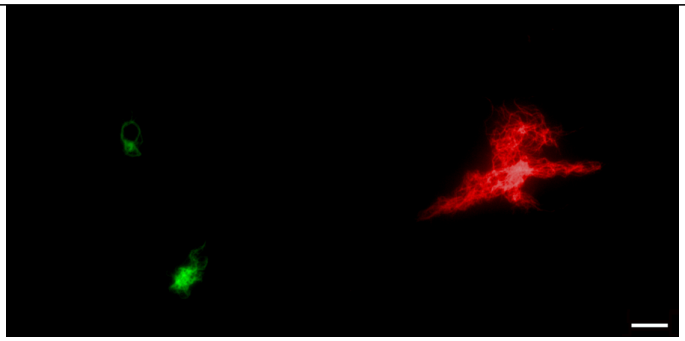	tubes and tangles 10-50μm 2 fields of view
7C 10x 10mg/mL	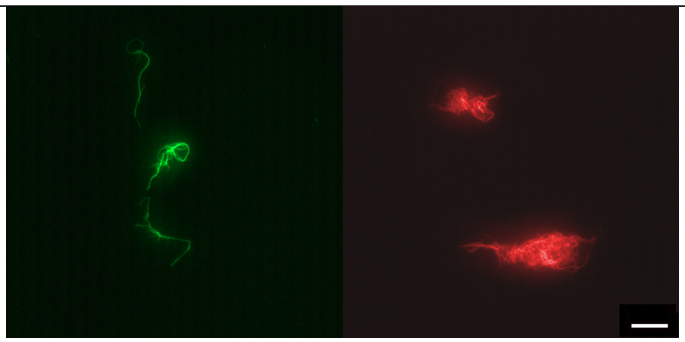	tubes and tangles 10-30μm 1 field of view
7C 1/3x 50mg/mL	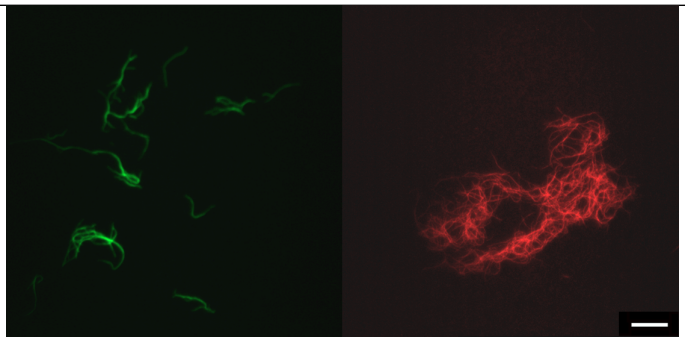	tangles and bifurcations 20-60μm 0.5 fields of view

6CA2 10x 5mg/mL	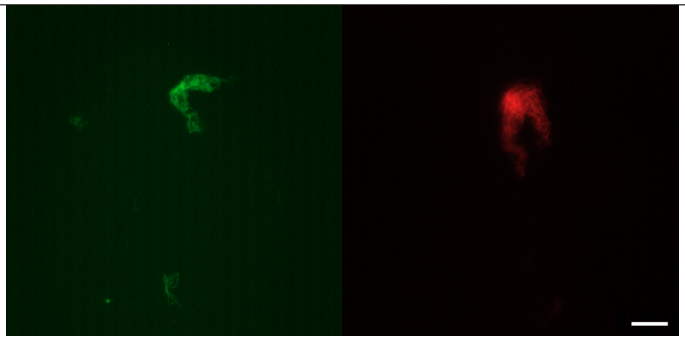	tubes and tangles 10-15μm 3 fields of view
6CA2 1/3x 50mg/mL	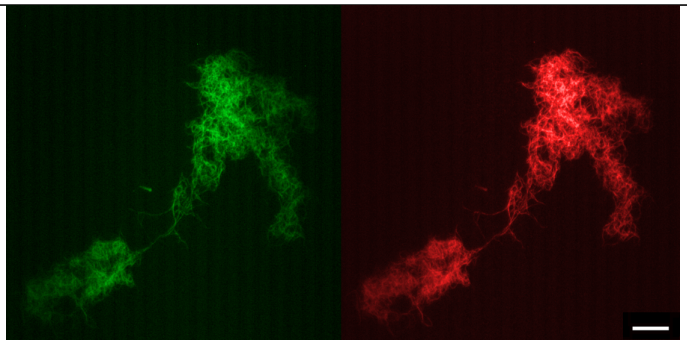	tangles 20-70μm 0.5 fields of view